Correlation between ground state and orbital anisotropy in heavy fermion materials

Thomas Willers[a], Fabio Strigari[a], Zhiwei Hu[b], Violetta Sessi[c], Nicholas B. Brookes[c], Eric D. Bauer[d], John L. Sarrao[d], J. D. Thompson[d], Arata Tanaka[e], Steffen Wirth[b], Liu Hao Tjeng[b], and Andrea Severing[a,1]

[a]Institute of Physics II, University of Cologne, 50937 Cologne, Germany; [b]Max Planck Institute for Chemical Physics of Solids, 01187 Dresden, Germany; [c]European Synchrotron Radiation Facility, 38043 Grenoble Cédex, France; [d]Los Alamos National Laboratory, Los Alamos, NM 87545; and [e]Department of Quantum Matter, Graduate School of Advanced Sciences of Matter, Hiroshima University, Higashi-Hiroshima 739-8530, Japan

Edited by G. Kotliar, Rutgers University, Piscataway, NJ, and accepted by the Editorial Board January 15, 2015 (received for review August 15, 2014)

The interplay of structural, orbital, charge, and spin degrees of freedom is at the heart of many emergent phenomena, including superconductivity. Unraveling the underlying forces of such novel phases is a great challenge because it not only requires understanding each of these degrees of freedom, it also involves accounting for the interplay between them. Cerium-based heavy fermion compounds are an ideal playground for investigating these interdependencies, and we present evidence for a correlation between orbital anisotropy and the ground states in a representative family of materials. We have measured the 4*f* crystal-electric field ground-state wave functions of the strongly correlated materials $CeRh_{1-x}Ir_xIn_5$ with great accuracy using linear polarization-dependent soft X-ray absorption spectroscopy. These measurements show that these wave functions correlate with the ground-state properties of the substitution series, which covers long-range antiferromagnetic order, unconventional superconductivity, and coexistence of these two states.

heavy fermions | crystal fields | X-ray absorption | rare earth

Why do many chemically and structurally highly similar compounds develop different ground states? This seemingly simple question still eludes a straightforward description despite intense research. However, it is specifically pressing in view of the quest for a deeper insight into unconventional superconductivity.

We here investigate heavy fermion metals, i.e., rare earth or actinide materials, in which a plethora of phenomena including antiferromagnetism and unconventional superconductivity can be observed. In these compounds, the *f* electrons hybridize with the conduction electrons (*cf* -hybridization), and, in analogy to the Kondo effect in diluted systems, the local magnetic moments can be screened in these so-called "Kondo lattices" at sufficiently low temperatures. However, the Kondo effect competes with the Ruderman–Kittel–Kasuya–Yosida interaction, which typically favors long-range magnetic order. As a result of this competition, a quantum phase transition from magnetically ordered to paramagnetic, more itinerant *f* electron behavior can take place. The balance of both interactions can be tuned by external parameters such as pressure, magnetic field, or doping (1). Non-Fermi liquid behavior and, of interest here, unconventional superconductivity often occur in the vicinity of such quantum critical points. However, despite research over the last 30 y, the ability to predict conditions favorable for superconductivity has remained elusive. Here, the cerium-115 family $CeMIn_5$ with M = Co, Ir, and Rh is ideally suited for a systematic study because ground states and changes in Fermi volumes in this family can be tuned easily by substitutions of one M element for another (2–25).

These heavy fermion compounds $CeMIn_5$ crystallize in the tetragonal $HoCoGa_5$-type structure as depicted in Fig. 1, with In1 being the in-plane and In2 the out-of-plane indium. Fig. 2 shows the substitution phase diagram of $CeRhIn_5$, where Rh is substituted by Ir or Co (5, 8–10, 12–15). For clarity, we show the magnetically ordered and superconducting regions on separate scales (up and down, respectively). $CeCoIn_5$ and $CeIrIn_5$ are superconductors with transition temperatures of T_c = 2.3 and 0.4 K (6, 7). $CeRhIn_5$, however, orders antiferromagnetically at T_N = 3.8 K. The magnetic order of $CeRhIn_5$ is incommensurate [incommensurate antiferromagnetically ordered (IC AF)] with the magnetic moments aligned in the *ab* plane, propagating in a spiral along the tetragonal *c* axis (3). Substituting Rh with Ir or Co tunes the ground state away from magnetic ordering toward bulk superconductivity by passing through regions where magnetic order and superconductivity coexist, and where—in the case of Ir substitution—a second commensurate magnetic phase has been observed (10). A commensurate phase has also been observed on the Co side, but here the coexistence with the incommensurate order is still a matter of debate, possibly due to uncertainties of the samples' stoichiometry (12–15). We note that the Fermi surface of $CeRhIn_5$ resembles that of $LaRhIn_5$, i.e., the 4*f* electron of Ce remains localized and does not contribute to the Fermi surface volume, in contrast to the Ir and Co samples, which show enlarged Fermi surfaces volumes, implying a more itinerant *f* electron behavior (18–22, 25), especially in the regions of pure superconductivity (23, 24).

On the search for interdependencies of physical parameters and ground-state properties, Bauer et al. (26) speculated about a linear relationship between lattice anisotropy c/a (here a and c are the lattice constants) and the superconducting transition temperature T_c for the superconducting plutonium and cerium-115 compounds. We, however, can see from Fig. 2 that this relationship does not hold for almost one-half of the phase diagram. The colored squares in Fig. 2 show the lattice anisotropy c/a

Significance

The ground state of materials with strong electronic correlations depends on a delicate balance among competing interactions. The strongly correlated compounds $CeMIn_5$, with M = Co, Rh, and Ir, exhibit superconducting and magnetic ground states as well as Fermi surface changes upon substituting one M element for another and become even higher temperature superconductors when Ce is substituted by Pu. They are therefore recognized as important model systems in which a search for parameters correlating with the occurrence of these ground states could be successful. The present X-ray absorption study of $CeRh_{1-x}Ir_xIn_5$ reveals that anisotropy of the Ce 4*f*-wave function is a significant parameter that is highly sensitive to the ground-state formation and should be taken into account when modeling these systems.

Author contributions: L.H.T. and A.S. designed research; T.W., F.S., Z.H., V.S., N.B.B., and A.S. performed research; E.D.B., J.L.S., and J.D.T. contributed new reagents/analytic tools; T.W., F.S., A.T., and A.S. analyzed data; and F.S., E.D.B., J.L.S., J.D.T., S.W., L.H.T., and A.S. wrote the paper.

The authors declare no conflict of interest.

This article is a PNAS Direct Submission. G.K. is a guest editor invited by the Editorial Board.

Freely available online through the PNAS open access option.

[1]To whom correspondence should be addressed. Email: severing@ph2.uni-koeln.de.

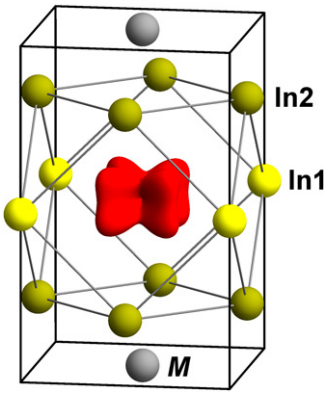

Fig. 1. Structure of Ce*M*In$_5$. The Ce atom is represented by the angular distribution of the 4*f* CEF ground-state orbital (red). The In1 (yellow), In2 (dark yellow), and the transition metal *M* (gray) are labeled in the figure.

(or rather a/c) on top of the $CeRh_{1-y}Co_yIn_5$–$CeRh_{1-x}Ir_xIn_5$ phase diagram. The a/c ratios are calculated from the values given in ref. 8 (orange squares) and ref. 5 (red squares), and in the following we will refer to a/c only as lattice anisotropy. Fig. 2 shows that Bauer et al.'s scaling works rather well in the purely superconducting regions. However, for magnetically ordered, Rh-rich samples, this linear dependency of T_c on a/c obviously breaks down. A closer inspection reveals that even in the region of phase coexistence there are significant deviations from a linear dependency ($CeRh_{1-x}Ir_xIn_5$ with $0.3 \leq x \leq 0.45$). Consequently, the lattice anisotropy has no predictive power concerning the formation of a superconducting ground state, motivating us to look further for a more fundamental parameter. In the following, we concentrate on the $CeRh_{1-x}Ir_xIn_5$ substitution series because the phase diagram is well defined (Fig. 2).

The importance of momentum-dependent hybridization and the impact of the anisotropic crystal-electric field (CEF) ground-state wave functions have been discussed by several groups (27–31). For the heavy fermion compound $CeIrIn_5$, Shim et al. (32) have even made specific predictions on the basis of first-principle dynamical mean field theory calculations. In particular, their calculations claim that the out-of-plane hybridization with the In2 ions is stronger than the in-plane one. These theoretical findings of anisotropic hybridization should be reflected in the CEF potential, implying a systematic change of the CEF wave function with hybridization and, consequently, with the ground-state properties. However, such an impact of the CEF wave function on the ground-state properties has never been proven experimentally, most likely due to the lack of accuracy of common methods. Here, we present results of a systematic investigation of the CEF ground states and the different ground state properties of $CeRh_{1-x}Ir_xIn_5$ using the soft X-ray absorption technique, which specifically targets the 4*f* ground-state wave function.

Results

Soft X-Ray Absorption Spectroscopy and Choice of Samples. We recently started using soft X-ray absorption spectroscopy (XAS) at the rare earth *M*-edges as a method for measuring CEF ground-state wave functions in heavy fermion compounds (33–35). Here, the dipole selection rules for linearly polarized light provide the sensitivity to the ground-state symmetry and allow its determination with unprecedented accuracy. The knowledge of excited CEF states is not required for the ground-state analysis as long as the data are taken at low enough temperatures; nor are data statistics or background hampering the result. This is a great advantage over more conventional methods like inelastic neutron scattering and single-crystal susceptibility.

We have chosen the Ir concentrations $x = 0$, 0.2, 0.3, 0.5, 0.75, and 1 of the $CeRh_{1-x}Ir_xIn_5$ series for the linear polarized soft XAS experiment. Here, $x = 0$ and 0.2 cover the purely incommensurate antiferromagnetic region of the phase diagram with an almost identical T_N. The region of phase coexistence, which comprises an incommensurate, a commensurate, and a superconducting state, is covered with the $x = 0.3$ and 0.5 samples. We note that, in both magnetic phases, the magnetic moments are aligned antiferromagnetically in the basal plane and that the region of phase coexistence has been discussed in detail in ref. 16. The magnetic order decays rapidly with further increasing Ir concentration so that the samples with $x = 0.75$ and 1 are purely superconducting. By this choice, we cover all phases of interest with two samples each for our systematic investigation of the orbital anisotropy.

XAS Data of $CeRh_{0.8}Ir_{0.2}In_5$. As an example, the top of Fig. 3 shows the total-electron-yield (TEY) intensities of the cerium M_4 and M_5 edge of $CeRh_{0.8}Ir_{0.2}In_5$ for the two polarizations $E \perp c$ (blue) and $E \parallel c$ (red) at T = 8 K. This temperature is low enough to assure excited CEF states are not populated ($\Delta E_1 \sim 70$ K and $\Delta E_2 \sim 230$ K) (34, 36, 37), so that the clear difference between the two polarizations is representative for the out-of-plane anisotropy of the ground-state orbital. The green dots in Fig. 3, *Bottom*, present the resulting linear dichroism (LD) in a 10-fold enlargement. The LD is the difference of the intensities for $E \perp c$ and $E \parallel c$. The data were then analyzed with an ionic full multiplet calculation (*Materials and Methods*, *Analysis*).

The CEF ground state in this compound family is a Γ_7 Kramer's doublet (34, 36, 37) and can be expressed in terms of J_z as follows:

$$\Gamma_7 = \alpha|\pm 5/2\rangle + \sqrt{1-\alpha^2}|\mp 3/2\rangle.$$

The quantity α^2 determines the out-of-plane anisotropy where $\alpha^2 > 1/6$ ($\alpha^2 < 1/6$) corresponds to a more oblate (prolate) 4*f* orbital. We find that a Γ_7 ground state with $\alpha^2 = 0.387 \pm 0.005$ describes the data (Fig. 3, *Middle*), and in particular the LD

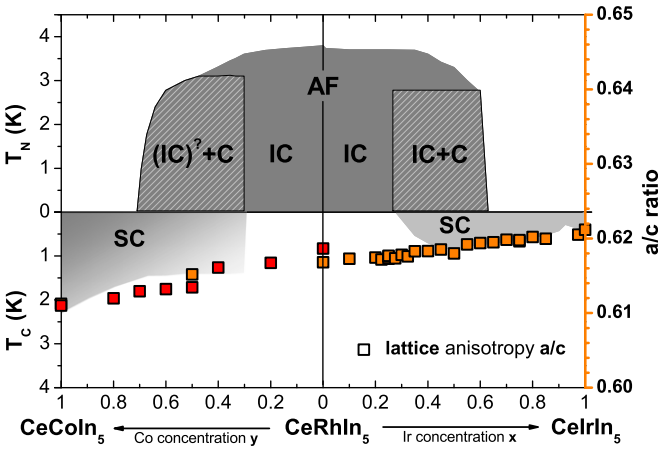

Fig. 2. Phase diagram of $CeRh_{1-x}Ir_xIn_5$ and $CeRh_{1-y}Co_yIn_5$, as adapted from refs. 5, 8–10, and 12–15, showing the magnetically ordered and superconducting regions as function of the Ir and Co concentration. The incommensurate antiferromagnetic ordered phases (IC AF) and the commensurate ones (C AF) are colored dark gray and hatched gray, respectively, and the regions of superconductivity (SC) are marked light gray. The question mark on the Co side refers to the ongoing discussion concerning the coexistence of IC and C AF order. The temperature scales of T_N and T_c are shown separately, the former one pointing up, and the latter one pointing down. The colored squares show the lattice anisotropy a/c (right scale) for $CeRh_{1-x}Ir_xIn_5$ and $CeRh_{1-y}Co_yIn_5$. The lattice constants *a* and *c* are taken from ref. 8 (orange squares) and ref. 5 (red squares).

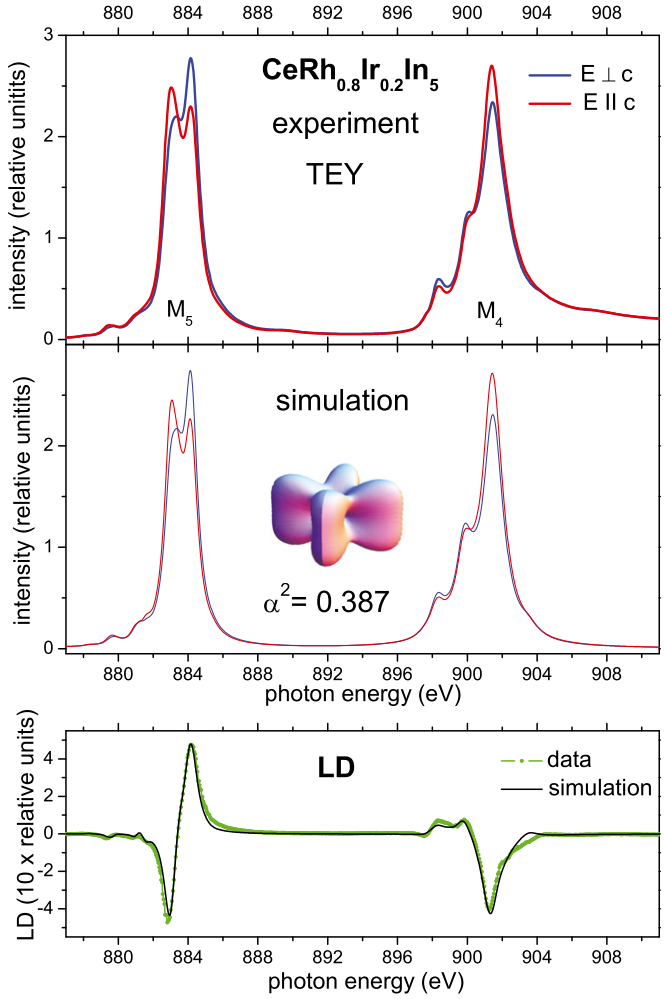

Fig. 3. Measured (*Top*) and simulated (*Middle*) linearly polarized XAS spectra of $CeRh_{0.8}Ir_{0.2}In_5$ at the $M_{4,5}$ edges at $T = 8$ K. The red spectra refer to measurements and simulations with E ∥ c and the blue ones with E ⊥ c. The *Inset* in the *Middle* shows the corresponding 4*f* spatial distribution. The panel at the *Bottom* compares the measured (green dots) and simulated LD (black line) enlarged by a factor of 10.

(black line in the panel at *Bottom*), very well. The *Inset* visualizes the corresponding 4*f* orbital. Note that dipole experiments like inelastic neutron scattering or soft XAS determine α^2, so that the sign of α cannot be determined.

Linear Dichroism of All Compositions. The results for the other Ir concentrations, which were obtained in the same manner, are summarized in Fig. 4. In the top panels of Fig. 4, the measured LD of both edges is depicted for the entire series of $CeRh_{1-x}Ir_xIn_5$ from $x = 0$–1. The LD is largest for the two Rh rich concentrations $x = 0$ and 0.2 (red and orange dots). It then decreases rapidly for the intermediate Ir concentration $x = 0.3$ (light green) and even more so for $x = 0.5$ (dark green). The LD is smallest and almost the same on the Ir-rich side ($x = 0.75$ and 1, light and dark blue dots). The lower panels of Fig. 4 exhibit the corresponding simulated LD, which reproduce nicely the measured strong reduction of the LD with increasing Ir concentration. The resulting orbital anisotropies α^2 are listed in Table 1. It is important to note that the LD of the interim compositions cannot be simulated with the respective fractions of the LD of $CeRhIn_5$ and $CeIrIn_5$. This is most obvious for $CeRh_{0.5}Ir_{0.5}In_5$, where $0.5\ LD_{CeRhIn_5} + 0.5\ LD_{CeIrIn_5}$ would yield an $\alpha^2 = 0.321$, whereas a value of 0.284 has been observed. This change of LD indicates that the CEF ground-state wave function changes monotonically, but not linearly with the Ir concentration, unlike the lattice anisotropy in Fig. 2. For completeness, we also give the value for $CeCoIn_5$ in Table 1 (34).

Discussion

Orbital Anisoptroy α^2 and Phase Diagram. In Fig. 5, the α^2 values are plotted as red circles along with the $CeRh_{1-x}Ir_xIn_5$ phase diagram for illustrating the changes of the wave function with the Ir concentration. The size of the circles corresponds to the error bars. As shown in Fig. 5, we now can observe a clear trend between the value of α^2 and the ground-state properties of $CeRh_{1-x}Ir_xIn_5$. The IC AF samples $CeRhIn_5$ and $CeRh_{0.8}Ir_{0.2}In_5$ on the Rh-rich side have almost the same large LD (Fig. 4), yielding the largest α^2 values within the series; the α^2 value of the $x = 0.2$ sample being only 5% smaller than the one of the pure Rh compound. In the intermediate region where the three phases coexist, α^2 decreases rapidly with x. On the Ir-rich side of the phase diagram, in the purely superconducting region, α^2 is small and levels off, i.e., it is identical for $CeRh_{0.25}Ir_{0.75}In_5$ and $CeIrIn_5$.

Apparently, the superconducting compositions favor the orbitals with smaller α^2 values. This becomes even more evident when taking into account $CeCoIn_5$: The α^2 value of $CeCoIn_5$ is smallest while it has the highest T_c (Fig. 5). Actually, its α^2 value falls rather nicely onto the phase diagram when using the same scaling as for the $CeRh_{1-x}Ir_xIn_5$ substitution series. This strongly supports our conjecture that α^2 is a parameter that correlates with the magnetic

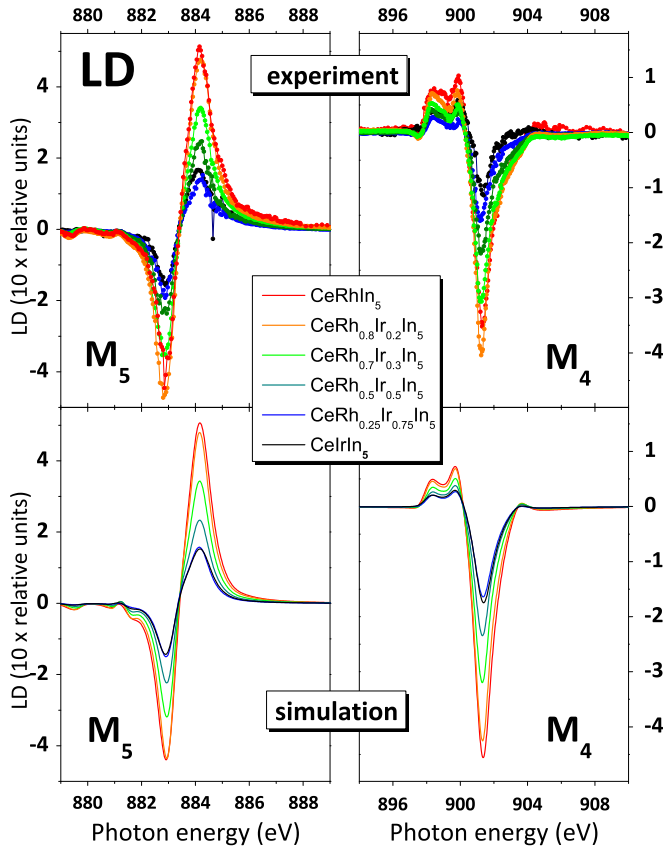

Fig. 4. The top panels show the experimental linear dichroism (LD) at the M_5 and M_4 edge for the Ir substitutions $x = 0.2$, 0.3, 0.5, and 0.75 in $CeRh_{1-x}Ir_xIn_5$ at 8 K. Data for $x = 0$ and 1 were taken in a previous experiment (34). The bottom panels show the corresponding simulations, which reproduce the data very well.

Table 1. Out-of-plane orbital anisotropy α^2 ($\Delta\alpha^2 = \pm 0.005$) for all measured Ir concentrations x in $CeRh_{1-x}Ir_xIn_5$ and for $CeCoIn_5$ from the present analysis

	Sample/Ir concentration x						
	$CeRIn_5$	$CeRh_{1-x}Ir_xIn_5$				$CeIr_xIn_5$	$CeCoIn_5$
Parameters	0	0.2	0.3	0.5	0.75	1	
α^2	0.407	0.387	0.328	0.284	0.242	0.242	0.123
Ce-In1 (Å)	3.292	—	—	—	—	3.305	3.262
Ce-In2 (Å)	3.278	—	—	—	—	3.272	3.283

Note that $\alpha^2 = 1/6 \approx 0.166$ would correspond to a cubic-type orbital. Ce-In1 and Ce-In2 are the distances between cerium and the in-plane (In1) and out-of-plane indium (In2) as taken from ref. 39.

as well as the superconducting phases, in contrast to a/c, which only serves the superconducting samples.

The implication of the changing J_z contribution on the spatial distribution of the 4f electrons in the CEF ground state is obvious when recalling that the pure $J_z = |\pm 5/2\rangle$ is donut shaped, whereas the pure $|\pm 3/2\rangle$ is yo-yo shaped (33). Upon going from $CeRhIn_5$ to $CeIrIn_5$, the orbital extends increasingly out-of-plane (Fig. 5) such that it becomes less oblate with increasing Ir concentration. For $CeCoIn_5$ the 4f orbital is prolate, i.e., has the largest extension in the c direction, and $CeCoIn_5$ has the highest superconducting transition temperature. We discuss possible correlations and implications in the following.

Intuitively, one would expect that the lattice anisotropy follows the orbital anisotropy, a behavior that has been observed, e.g., in the Ce-monopnictides (38). However, in the $CeMIn_5$ family, this is obviously not the case. Although the lattice constants of the $CeRh_xIr_{1-x}In_5$ series nicely follow Vegard's law (8), so that the "lattice" anisotropy a/c in Fig. 2 changes accordingly with the Ir concentration, the "orbital" anisotropy α^2 changes in a strongly nonlinear manner (Fig. 5). Furthermore, while the unit cell becomes shorter along the c axis from Rh to Ir, the 4f orbital extends increasingly out of the ab plane, suggesting an anticorrelation, rather than a correlation, between the 4f wave function's "flatness" and the a/c ratio. However, $CeCoIn_5$ indicates the opposite (i.e., correlating) behavior: in this compound, the 4f orbital is the most extended one along c, whereas the smallest a/c ratio (largest c/a) is observed. Apparently, there is no obvious systematics between orbital and lattice anisotropy (compare Figs. 2 and 5).

We now focus on the orbital angular distribution with respect to the degree of cf-hybridization in this compound family. We emphasize that the degree of hybridization has been measured by independent experiments. The stronger cf-hybridization of the superconducting compounds $CeIrIn_5$ and $CeCoIn_5$ is reflected in a larger Fermi surface (18–22, 25) and also in a larger quasielastic line width. Inelastic neutron scattering on powder samples found a line width of half-width at half-maximum ~1.4 meV for the magnetically ordering Rh compound and line widths at least twice as large for $CeIrIn_5$ and $CeCoIn_5$ (34). The importance of direction-dependent hybridization is an obvious consequence when combining the two experimental findings of cf-hybridization strength and angular distribution of the CEF wave function. The taller orbitals are more strongly hybridized. This is in agreement with the theoretical conjecture by Shim et al. (32) that the out-of-plane hybridization with the In2 ions is most important despite nearly identical Ce–In bond lengths [Table 1 (39)], thus providing a channel for the In2–M interaction to contribute significantly to the total electronic energy minimization. This yields a natural explanation for why the physical properties depend so much on the transition metal atoms. As a consequence of the anisotropic hybridization, the shape of the CEF wave function, i.e., the parameter α^2, marks whether a compound is more itinerant and possibly superconducting, or more localized and antiferromagnetic.

How does this relate to the observed (26) linear correlation between the lattice anisotropy a/c and T_c for the superconducting plutonium and cerium-115 compounds? We already noted that this correlation only holds for the superconducting compositions, so that the a/c ratio by itself cannot be used to predict whether or not a compound becomes superconducting. For example, the a/c ratio of $CeRhIn_5$ would indicate a finite T_c at ambient pressure, whereas experimentally no superconductivity has been recorded (Fig. 2). Here, we infer that α^2 is the parameter that distinguishes superconducting from nonsuperconducting compounds. Once the purely superconducting region of the phase diagram has been reached, α^2 does not change any more and the a/c ratio seemingly tunes T_c.

Summary. The CEF ground-state wave functions of the $CeRh_{1-x}Ir_xIn_5$ substitution series have been determined, and a clear correlation between ground-state properties and wave functions has been observed. These findings suggest that the shape of the cerium wave function—expressed through the parameter α^2—serves as a good predictor of whether a given material becomes superconducting or magnetic. More generally, anisotropic hybridization must be a necessary component in an appropriate description of Kondo lattice materials and of the evolution of their ground states as a function of a nonthermal tuning parameter.

Materials and Methods

Samples. High-quality single crystals of $CeRh_{1-x}Ir_xIn_5$ were grown by flux growth and well characterized by magnetic susceptibility and/or heat capacity to ensure their nominal composition is in accordance with the phase diagram (8, 10). Before the absorption experiment, all crystals were aligned within 1–2° by Laue X-ray diffraction.

Method. The linearly polarized soft XAS experiment was performed at the European Synchrotron Radiation Facility in Grenoble, France, at the ID08 undulator beamline. We recorded the Ce M-edge absorption spectra in the TEY mode. The energy resolution at the $M_{4,5}$ edges ($h\nu \approx 875-910$ eV) was set to 0.2 eV. The samples were cleaved in situ in an ultrahigh-vacuum chamber with a pressure of 2×10^{-10} mbar at 8 K. The $M_{4,5}$ edges were recorded for light polarized parallel (E ∥ c) and perpendicular (E ⊥ c) to the tetragonal c axis. Here, the undulator beamline has the advantage that, for

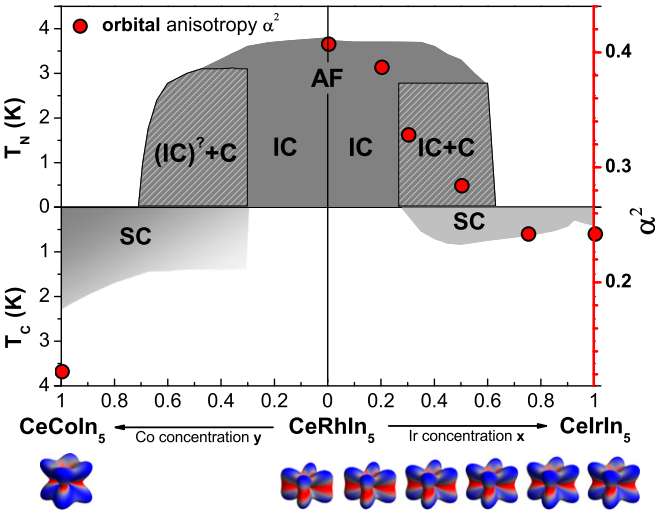

Fig. 5. Orbital anisotropy α^2 on the right scale as function of x in $CeRh_{1-x}Ir_xIn_5$ and for $CeCoIn_5$. The evolution with x of the angular distributions of the 4f CEF ground-state orbitals in $CeRh_{1-x}Ir_xIn_5$ and $CeCoIn_5$ is shown below the phase diagram.

normal incidence, the polarization can be changed without moving the sample, so that the same sample spot is probed for both polarization directions. For each sample, different spots were probed to rule out sample inhomogeneities. The data of $CeRh_{1-x}Ir_xIn_5$ were taken at 8 K for the four Ir substitutions, $x = 0.2$, 0.3, 0.5, and 0.75. The excited CEF states are above 5 meV (~50 K) (34, 36, 37) so that at 8 K only the ground state is probed. The data of $CeRhIn_5$ ($x = 0$), $CeIrIn_5$ ($x = 1$), and also of $CeCoIn_5$ were taken in a previous experiment (34). For the data analysis, all data were normalized to the intensity of the isotropic spectra $I_{iso} = (2I_{E\perp c} + I_{E\|c})/3$.

Analysis. The XAS data have been simulated with ionic full multiplet calculations based on the XTLS 8.3 program (40). The atomic parameters are given by reduced Hartree–Fock values. The reduction accounts for the configuration interaction, which is not included in the Hartree–Fock calculations and is determined from fitting the isotropic spectra I_{iso}. Typical reductions are about 40% for the 4*f*–4*f* Coulomb interactions and about 20% for the 3*d*–4*f* interactions (33–35). In the present manuscript, the LD of the end members of the series were analyzed in the same manner as for the substitution series investigated here.

ACKNOWLEDGMENTS. We thank P. Thalmeier for fruitful discussions. The wave function density plots were calculated using the CrystalFieldTheory package for Mathematica written by M. W. Haverkort. Support from the German funding agency Deutsche Forschungsgemeinschaft under Grant 583872 is gratefully acknowledged. Work at Los Alamos National Laboratory was performed under the auspices of the US Department of Energy, Office of Basic Energy Sciences, Division of Materials Sciences and Engineering.

1. Gegenwart P, Si Q, Steglich F (2008) Quantum criticality in heavy fermion metals. *Nat Phys* 4:186–197.
2. Hegger H, et al. (2000) Pressure-induced superconductivity in quasi-2D $CeRhIn_5$. *Phys Rev Lett* 84(21):4986–4989.
3. Bao W, et al. (2000) Incommensurate magnetic structure of $CeRhIn_5$. *Phys Rev B* 62(22):R14621–R14624.
4. Bao W, et al. (2003) Erratum: Incommensurate magnetic structure of $CeRhIn_5$. *Phys Rev B* 67(9):099903.
5. Zapf VS, et al. (2001) Coexistence of superconductivity and antiferromagnetism in $CeRh_{1-x}Co_xIn_5$. *Phys Rev B* 65(1):014506.
6. Petrovic C, et al. (2001) Heavy-fermion superconductivity in $CeCoIn_5$ at 2.3 K. *J Phys Condens Matter* 13(17):L337.
7. Petrovic C, et al. (2001) A new heavy-fermion superconductor $CeIrIn_5$: A relative of the cuprates? *Europhys Lett* 53(3):354–359.
8. Pagliuso PG, et al. (2001) Coexistence of magnetism and superconductivity in $CeRh_{1-x}Ir_xIn_5$. *Phys Rev B* 64(10):100503.
9. Pagliuso PG, et al. (2002) Multiple phase transitions in Ce(Rh,Ir,Co)In_5. *Physica B* 312-313:129–131.
10. Llobet A, et al. (2005) Novel coexistence of superconductivity with two distinct magnetic orders. *Phys Rev Lett* 95(21):217002.
11. Park T, et al. (2006) Hidden magnetism and quantum criticality in the heavy fermion superconductor $CeRhIn_5$. *Nature* 440(7080):65–68.
12. Ohira-Kawamura S, et al. (2007) Competition between unconventional superconductivity and incommensurate antiferromagnetic order in $CeRh_{1-x}Co_xIn_5$. *Phys Rev B* 76(13):132507.
13. Ohira-Kawamura S, et al. (2008) Neutron diffraction study on heavy fermion superconducting and antiferromagnetic compounds $CeRh_{1-x}Co_xIn_5$. *Phys Stat Sol A* 2016(5): 1076–1081.
14. Yokoyama M, et al. (2008) Change of antiferromagnetic structure near a quantum critical point in $CeRh_{1-x}Co_xIn_5$. *Phys Rev B* 77(22):224501.
15. Yokoyama M, et al. (2008) Polarized neutron scattering study on antiferromagnetic states in $CeRh_{0.6}Co_0.4In_5$. *Physica B* 403(5-9):812–814.
16. Thompson JD, Fisk Z (2012) Progress in heavy-fermion superconductivity: Ce115 and related materials. *J Phys Soc Jpn* 81(1):011002.
17. Aynajian P, et al. (2012) Visualizing heavy fermions emerging in a quantum critical Kondo lattice. *Nature* 486(7402):201–206.
18. Haga Y, et al. (2001) Quasi-two-dimensional Fermi surfaces of the heavy fermion superconductor $CeIrIn_5$. *Phys Rev B* 63(6):060503.
19. Fujimori SI, et al. (2003) Nearly localized nature of *f* electrons in Ce*T*In_5 (*T* = Rh, Ir). *Phys Rev B* 67(14):144507.
20. Harrison N, et al. (2004) 4f-electron localization in CexLa 1-xM In5 with M=Co, Rh, or Ir. *Phys Rev Lett* 93(18):186405.
21. Shishido H, Settai R, Harima H, Onuki Y (2005) A drastic change of the Fermi surface at a critical pressure in $CeRhIn_5$: dHvA study under pressure. *J Phys Soc Jpn* 74(4):1103–1106.
22. Settai R, Takeuchi T, Onuki Y (2007) Recent advances in Ce-based heavy fermion superconductivity and Fermi surface properties. *J Phys Soc Jpn* 76(5):051003.
23. Shishido H, Settai R, Kawai T, Harima H, Onuki Y (2007) de Haas-van Alphen effect of $CeIr_{1-x}Rh_xIn_5$. *J Magn Magn Mater* 310(2):303–304.
24. Goh SK, et al. (2008) Fermi-surface reconstruction in $CeRh_{1-x}Co_xIn_5$. *Phys Rev Lett* 101(5):056402.
25. Allen MP, et al. (2013) Imaging Cooper pairing of heavy fermions in $CeCoIn_5$. *Nat Phys* 9:468–473.
26. Bauer ED, et al. (2004) Structural tuning of unconventional superconductivity in PuMGa5 (M=Co,Rh). *Phys Rev Lett* 93(14):147005.
27. Pagliuso PG, et al. (2002) Structurally tuned superconductivity in heavy-fermion Ce-MIn_5 (*M* = Co, Ir, Rh). *Physica B* 320(1-4):370–375.
28. Thalmeier P, Zwicknagl G (2005) *Handbook on the Physics and Chemistry of Rare Earths*, eds Gschneider, Jr KA, Bünzli J-CG, Pecharsky VK (Elsevier, Amsterdam), Vol 34, pp 135–287.
29. Burch KS, et al. (2007) Optical signatures of momentum-dependent hybridization of the local moments and conduction electrons in Kondo lattices. *Phys Rev B* 75(5): 054523.
30. Haule K, Yee CH, Kim K (2010) Dynamical mean-field theory within the full-potential methods: Electronic structure of $CeIrIn_5$, $CeCoIn_5$, and $CeRhIn_5$. *Phys Rev B* 81(19): 195107.
31. Pourovskii LV, Hansmann P, Ferrero M, Georges A (2014) Theoretical prediction and spectroscopic fingerprints of an orbital transition in $CeCu_2Si_2$. *Phys Rev Lett* 112(10): 106407.
32. Shim JH, Haule K, Kotliar G (2007) Modeling the localized-to-itinerant electronic transition in the heavy fermion system $CeIrIn_5$. *Science* 318(5856):1615–1617.
33. Hansmann P, et al. (2008) Determining the crystal-field ground state in rare earth heavy fermion materials using soft-x-ray absorption spectroscopy. *Phys Rev Lett* 100(6):066405.
34. Willers T, et al. (2010) Crystal-field and Kondo-scale investigations of Ce*M*In_5 (*M*=Co, Ir, and Rh): A combined x-ray absorption and inelastic neutron scattering study. *Phys Rev B* 81(19):195114.
35. Strigari F, et al. (2012) Crystal-field ground state of the orthorhombic Kondo insulator $CeRu_2Al_{10}$. *Phys Rev B* 86(8):081105.
36. Christianson AD, et al. (2004) Crystalline electric field effects in Ce*M*In_5 (*M*=Co,Rh,Ir): Superconductivity and the influence of Kondo spin fluctuations. *Phys Rev B* 70(13): 134505.
37. Christianson AD, et al. (2002) Neutron scattering study of crystal fields in $CeRhIn_5$. *Phys Rev B* 66(19):193102.
38. Hannan A, et al. (2004) Exotic properties of CeSb studied by x-ray diffraction. *J Phys Soc Jpn* 73(7):1881–1887.
39. Moshopoulou EG, et al. (2002) Comparison of the crystal structure of the heavy-fermionmaterials $CeCoIn_5$, $CeRhIn_5$ and $CeIrIn_5$. *Appl Phys A* 74:s895–s897.
40. Tanaka A, Jo T (1994) Resonant 3*d*, 3*p* and 3*s* photoemission in transition metal oxides predicted at 2p threshold. *J Phys Soc Jpn* 63(7):2788–2807.